

# Sensitivity of an Imaging Space Infrared Interferometer

By

Tadashi NAKAJIMA\* and Hideo MATSUHARA†

(November 1, 2000)

**Abstract:** We study the sensitivities of space infrared interferometers. We formulate the signal-to-noise ratios of infrared images obtained by aperture synthesis in the presence of source shot noise, background shot noise and detector read noise. We consider the case in which  $n$  beams are pairwise combined at  $n(n-1)/2$  detectors and the case in which all the  $n$  beams are combined at a single detector. We apply the results to a future mission, Terrestrial Planet Finder. We also discuss the potential of a far-infrared interferometer for a deep galaxy survey.

## 1. INTRODUCTION

For the 2010's, space infrared interferometers such as Terrestrial Planet Finder (TPF) (TPF Science Working Group 1999) and Darwin (Penny et al. 1998) are considered with the emphasis on the detection of terrestrial planets around nearby stars. TPF and Darwin will be composed of several radiation cooled apertures and be capable of general synthesis imaging as well as planet detection by nulling interferometry. The detection limits of these interferometers for general purpose imaging are of great interest. However, no rigorous analyses of the sensitivities of these interferometers have been made, partly because there is no exact formula of the signal-to-noise ratio (SNR) of an infrared image made by aperture synthesis.

At optical wavelengths, the signal-to-noise ratios of synthesis images have been formulated by Prasad & Kulkarni 1989 (hereafter PK89) taking into account the source shot noise. Their formulae are not applicable at infrared wavelengths because of the presence of thermal background shot noise and detector read noise. We have expanded the work by PK89 and present the formulae of the SNRs of infrared synthesis images in this paper.

The beam combination geometry is a major issue in studying the sensitivity of an interferometer. One extreme is an  ${}^n C_2$  interferometer in which  $n$  beams are divided into  $n(n-1)$

---

\* National Astronomical Observatory, 2-21-1 Osawa, Mitaka, 181-8588, Japan;  
tadashi.nakajima@nao.ac.jp

† The Institute of Space and Astronautical Science, 3-1-1 Yoshinodai, Sagamihara, 229-8510, Japan;  
maruma@ir.isas.ac.jp

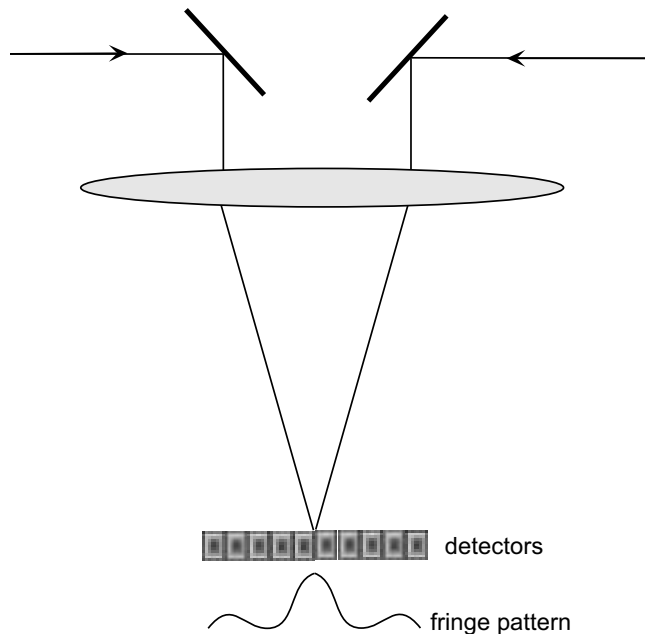


Fig. 1: Schematic diagram of a focal plane interferometer. There is one detector for each baseline.

subbeams and they are pairwise combined at  ${}^n C_2 = n(n-1)/2$  detectors. The other extreme is an  ${}^n C_n$  interferometer in which all the  $n$  beams are combined at  ${}^n C_n = 1$  detector.

While only spectrally narrow light was analyzed by PK89, we also consider spectrally broad light. In the case of spectrally broad light, whether fringes can be spectrally dispersed is an important issue. Fringe dispersion is always possible for the  ${}^n C_2$  interferometer. On the other hand, for the  ${}^n C_n$  interferometer, it is possible only for a one dimensional baseline configuration.

We present the formulae of SNRs for the  ${}^n C_2$  and  ${}^n C_n$  interferometers respectively in §2 and §3. We discuss the tradeoff between the two interferometers in §4. Capabilities of infrared interferometers for a deep survey are discussed in comparison with space observatories in §5.

## 2. ${}^n C_2$ INTERFEROMETER

Let there be  $n$  identical principal apertures from which we derive  $n$  main beams. Each beam is divided into  $n-1$  subbeams by the use of beam splitters. The resulting  $n(n-1)$  subbeams are combined pairwise at  $n_b = n(n-1)/2$  detectors where  $n_b$  is also the number of baselines. The fringe pattern is formed at the focal plane of each detector which is either a one dimensional array of identical pixels or a two dimensional array of identical pixels which range from 1 to  $P$  (Figure 1). For spectrally broad light, the fringe can be dispersed in the cross fringe direction with the use of a two dimensional detector. For a focal plane interferometer of this type, the influence of source shot noise on fringe phasor estimation has been fully formulated (Walkup & Goodman 1973; Goodman 1985). Let the interferometer be illuminated by a source and spatially smooth background. The intensity pattern on the  $r$ th detector ( $r$ th baseline) is given by

$$\langle I_r(\mathbf{x}) \rangle = 2 \langle I_0 \rangle \left[ 1 + \gamma_r \cos(\kappa \mathbf{x} \cdot \mathbf{B}_r/d + \phi_r) \right], \quad (1)$$

where  $\langle I_0 \rangle$  is the average intensity in each subbeam at the detector,  $\mathbf{B}_r$  is the baseline vector,  $\kappa = 2\pi/\lambda$  is the wave number, and  $d$  is the distance between the aperture plane and the detector,  $\mathbf{x}$  is the spatial vector in the detector plane, and  $\gamma_r \exp(i\phi_r)$  is the complex visibility function at the baseline vector  $\mathbf{B}_r$ . In deriving (1), we have assumed that the incident light is spectrally narrow so that the fringe visibility depends on only the spatial correlation of the field.

Because of the presence of background illumination,

$$I_0 = I_0^s + I_0^b, \quad (2)$$

where  $I_0^s$  and  $I_0^b$  are source and background intensities respectively. Let  $\gamma_r^s$  be the fringe visibility of the source in the absence of the background, then

$$\gamma_r = \frac{I_0^s}{I_0^s + I_0^b} \gamma_r^s. \quad (3)$$

The complex visibility function  $\gamma_r^s \exp(i\phi_r)$  is determined by the  $uv$  coordinates of the  $r$  th baseline ( $u, v$ ) and the source brightness distribution on the sky  $S(x, y)$  with the relation,

$$\gamma_r^s \exp(i\phi_r) = \frac{1}{\int S(x, y) dx dy} \int S(x, y) \exp\{-2\pi i(ux + vy)\} dx dy, \quad (4)$$

where symbols,  $S(x, y)$ ,  $u, v, x$ , and  $y$  are used only for this expression.

In an effort to reduce the clutter in the equations we henceforth drop the vector notation, but bear in mind that spatial frequencies, pixel locations, etc. are really vectors. The photoelectron detection theory (Walkup & Goodman 1973) takes into account the discrete nature of both photons and detector pixels. The average photoelectron count  $\langle k_r(p) \rangle$  at the pixel location specified by the integer index  $p$  of the detector is proportional to  $\langle I(x) \rangle$ :

$$\langle k_r(p) \rangle = 2 \langle K_0 \rangle \left[ 1 + \gamma_r \cos(p\omega_r + \phi_r) \right]. \quad (5)$$

Here,  $\langle \dots \rangle$  denotes averaging over the photoelectron-detection process. The product  $p\omega_r$  is understood to be the scalar product of the pixel position vector  $\mathbf{p}$  and the spatial frequency  $\omega_r$  expressed in inverse pixel units.

Let  $\langle C \rangle$  be the average number of photoelectrons detected by the entire array in one integration period, and let  $2\langle N \rangle$  be the average number of photoelectrons per detector per integration time. Clearly then,  $\langle C \rangle = 2\langle N \rangle n_b$ , and thus  $\langle N \rangle = \langle C \rangle / \{n(n-1)\}$ . According to (5), the average number of photoelectrons per detector is equal to  $2\langle K_0 \rangle P$ , and thus  $\langle K_0 \rangle P = \langle N \rangle$ .

An analysis based on the photodetection theory gives the mean image as follows.

$$\begin{aligned} I_1(q) &= \langle N \rangle \sum_r \gamma_r \cos(\omega_r q + \phi_r) \\ &= \langle N \rangle \sum_r \frac{I_0^s}{I_0^s + I_0^b} \gamma_r^s \cos(\omega_r q + \phi_r). \end{aligned} \quad (6)$$

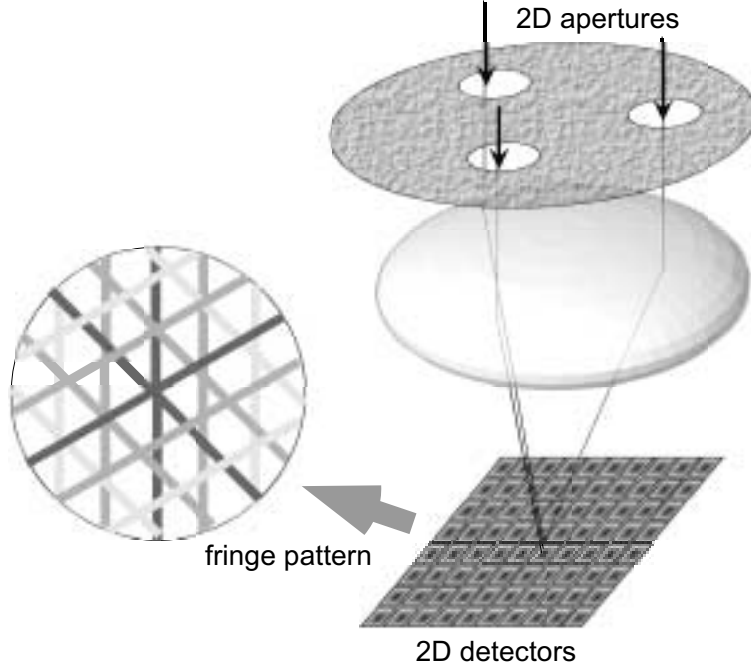


Fig. 2: Schematic diagram of a  ${}^3C_3$  interferometer. Beams from all apertures are superposed on a single detector.

The image  $I_1(q)$  is referred to as the dirty image in the parlance of radio astronomy. The dirty image is the convolution of the true image and the Fourier transform of the spatial frequency sampling function or the dirty beam. A synthesized image can be obtained from the dirty image by deconvolution.

The variance  $V[i_1(q)]$  in the synthesized image  $i_1(q)$  is given by

$$V[i_1(q)] = n_b \left( \langle N \rangle + \frac{P\sigma^2}{2} \right) = \frac{\langle C \rangle}{2} + n_b \frac{P\sigma^2}{2}. \quad (7)$$

Now we consider the specific case of a point source ( $\gamma_r^s = 1$ ) at the phase center ( $\phi_r = 0$ ) for which  $I_1(0) = \frac{\langle C \rangle}{2}$ . Since the source is located at the phase center, the SNR of the central pixel in the image is indicative of the SNR in the image:

$$\frac{I_1(0)}{\sqrt{V[i_1(0)]}} = \frac{(\langle C \rangle / 2) \{I_0^s / (I_0^s + I_0^b)\}}{\sqrt{\langle C \rangle / 2 + n_b P \sigma^2 / 2}}. \quad (8)$$

### 3. ${}^n C_n$ INTERFEROMETER

In the  ${}^n C_n$  interferometer, all the  $n$  beams interfere on a single detector and  $n_b$  fringes are superposed. Both the baseline configuration and the detector can be either one dimensional or two dimensional. As an example, a two dimensional  ${}^3 C_3$  interferometer is schematically presented in Figure 2. A special case is the combination of a one dimensional baseline configuration and a two dimensional detector for which the superposed fringes are dispersed in the

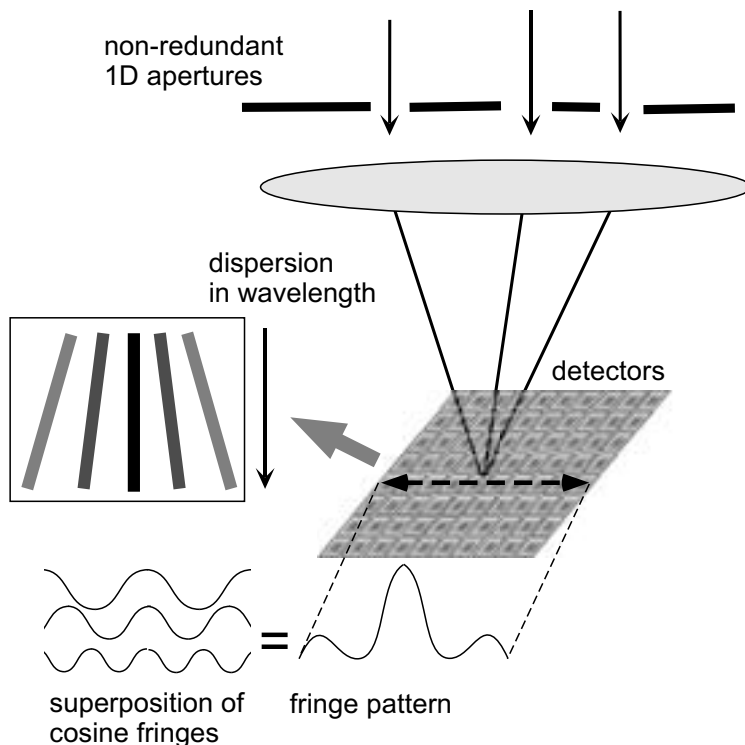


Fig. 3: Schematic diagram of a one-dimensional  ${}^3C_3$  interferometer. Fringes are spectrally dispersed in cross fringe direction.

cross fringe direction so that spectrally broad light can be used without bandwidth smearing (Figure 3).

Let the interferometer be composed of  $n$  identical apertures and let it be illuminated by a source and spatially smooth background. The classical intensity distribution of the interference pattern by the  $n$  apertures has the average value

$$\langle I(\mathbf{x}) \rangle = \langle I_0 \rangle \left[ n + 2 \sum_{g < h} \gamma_{gh} \cos(\kappa \mathbf{x} \cdot \mathbf{B}_{gh}/d + \phi_{gh}) \right], \quad (9)$$

where the various symbols have meanings similar to those in (1).  $gh$  denotes the baseline  $gh$  corresponding to the apertures  $g$  and  $h$ . Let  $\langle k(\mathbf{p}) \rangle$  denote the photoelectron count distribution due to  $\langle I(\mathbf{x}) \rangle$ . As in §2, we discontinue the vector notation, assume that the total number of pixels is  $P$ , and note that  $\langle k(p) \rangle$  is proportional to  $\langle I(x) \rangle$ :

$$\langle k(p) \rangle = \langle Q_0 \rangle \left[ n + \sum_{g < h} \gamma_{gh} \cos(p\omega_{gh} + \phi_{gh}) \right]. \quad (10)$$

Here  $\langle Q_0 \rangle$  has approximately the same meaning as  $\langle K_0 \rangle$  in §2. However, since there is no beam splitting,  $\langle Q_0 \rangle = (n - 1) \langle K_0 \rangle$ .

If we define  $\langle M \rangle = P \langle Q_0 \rangle = \langle C \rangle / n$ , we find the mean synthesized image to be

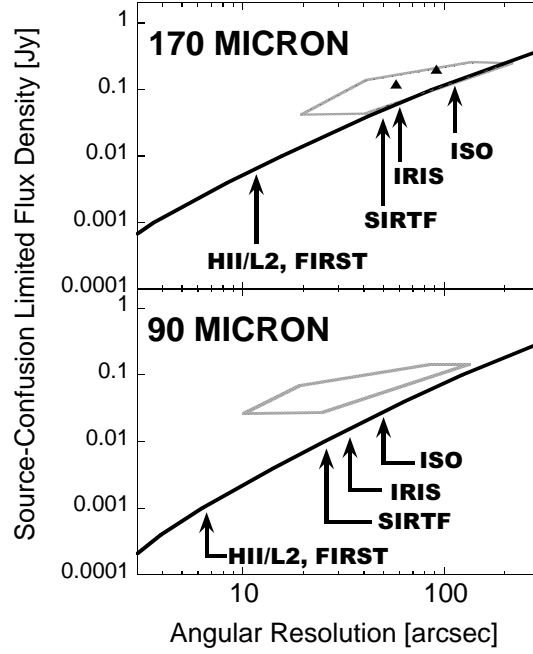


Fig. 4: Confusion limits of observatories. The confusion limits predicted from the model E of Guiderdoni et al. 1998 (solid line) are compared with those estimated from ISO observations by Matsuhara et al. 2000 (polygon) and Puget et al. 1999 (triangle).

$$I_2(q) = \langle M \rangle \sum_{i < j} \gamma_{ij} \cos(q\omega_{ij} + \phi_{ij}). \quad (11)$$

The variance  $V[i_2(q)]$  in the synthesized image  $i_2(q)$  is given by

$$V[i_2(q)] = \frac{n \langle M \rangle + P\sigma^2}{2} n_b + \langle M \rangle (n-2) \sum_{i < j} \frac{I_0^s}{I_0^s + I_0^b} \gamma_{ij}^s \cos(q\omega_{ij} + \phi_{ij}). \quad (12)$$

For a point source at the phase center,  $q = 0$ ,  $\gamma_{ij}^s = 1$ ,  $\phi_{ij} = 0$  and the SNR of the synthesized image is

$$\frac{I_1(0)}{\sqrt{V[i_1(0)]}} = \frac{\langle C \rangle \{I_0^s / (I_0^s + I_0^b)\} \sqrt{(n-1)/n}}{\sqrt{\langle C \rangle + P\sigma^2 + \langle C \rangle \{I_0^s / (I_0^s + I_0^b)\} \{2(n-2)/n\}}}. \quad (13)$$

#### 4. TRADEOFF BETWEEN ${}^n C_2$ AND ${}^n C_n$ INTERFEROMETERS

Using equations 8 and 13, the tradeoff between  ${}^n C_2$  and  ${}^n C_n$  interferometers can be investigated. Here we summarize the result of such a study. We denote a one-dimensional  ${}^n C_n$  interferometer as an  ${}^n C'_n$  interferometer.

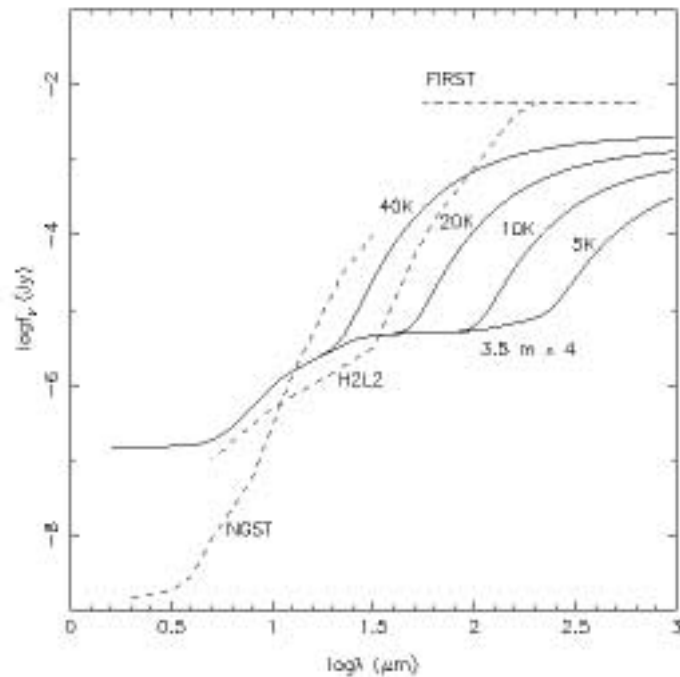


Fig. 5: Comparison with observatories. The sensitivity of an  ${}^n C_2$  interferometer composed of four 3.5 m apertures is plotted for telescope temperatures of 5, 10, 20, and 40 K with emissivity of 5%. The maximum baseline length is assumed to be 100 m. Dashed lines denote the sensitivities of NGST, HII/L2, and FIRST given for comparison.

In the background limit for spectrally narrow light, the  ${}^n C_n$  interferometer is preferred in this case. However the difference is at most by a factor  $\sqrt{2}$  for a large  $n$ .

In the background limit for spectrally broad light, the situation is more complicated. For a short baseline (small  $B/D$ ), the  ${}^n C_n$  interferometer is superior and for a long baseline, the  ${}^n C_2$  has an advantage. We can also compare the same one dimensional baseline configuration with different beam combination geometries. In this case, the  ${}^n C'_n$  interferometer is superior to the  ${}^n C_2$  interferometer at most by a factor  $\sqrt{2}$ .

In the read noise limit, there is a tradeoff. For a short baseline the  ${}^n C_n$  interferometer is superior and for a long baseline the  ${}^n C_2$  interferometer is better. For the same one dimensional baseline configuration, the  ${}^n C'_n$  interferometer is always superior to the  ${}^n C_2$  interferometer in the read noise limit.

In summary, for a practical use of long-baseline interferometry, the  ${}^n C'_n$  interferometer is the best for a one dimensional baseline configuration and  ${}^n C_2$  interferometer is better for a two dimensional baseline configuration.

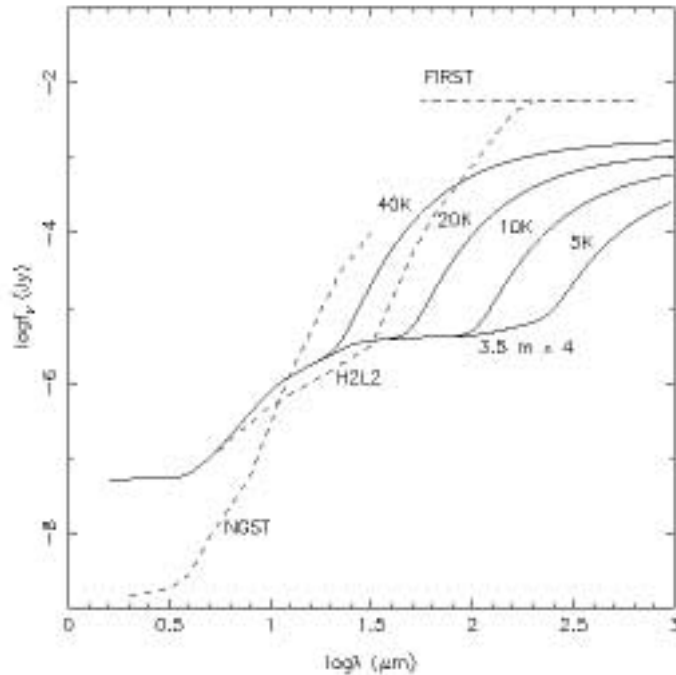


Fig. 6: Comparison with observatories. The sensitivity of a one dimensional  $^nC_n$  interferometer composed of four 3.5 m apertures is plotted for telescope temperatures of 5, 10, 20, and 40 K with emissivity of 5%. The maximum baseline length is assumed to be 100 m. Dashed lines denote the sensitivities of NGST, HII/L2, and FIRST given for comparison.

## 5. CAPABILITY FOR A DEEP FAR-INFRARED SURVEY AND COMPARISON WITH OBSERVATORIES

In this section, we investigate the potential of a TPF-like space interferometer for a deep far-infrared survey which is important in studying the galaxy formation history. At present, the deepest far-infrared galaxy counts are the ones by the ISO deep surveys of the Lockman hole (Kawara et al. 1998) and the Marano 1 field (Puget et al. 1999). The detection limits of individual sources at 90 and 170  $\mu\text{m}$  set by confusion are around 100 mJy and a fluctuation analysis extended the galaxy count down to 30 and 50 mJy respectively (Matsuhara et al. 2000). The galaxy counts have revealed strong evolution of star-forming galaxies from  $z = 0$  to 1 by a factor of 10 to 50. This excess of luminous low-redshift galaxies was not predicted by previous model calculations.

In Figure 4, source confusion limits at 90 and 170  $\mu\text{m}$  of different observatories predicted by the model E of Guiderdoni et al. (1998) are compared with those estimated from the recent ISO observations (Puget et al. 1999; Matsuhara et al. 2000). The model E of Guiderdoni et al. is known as one of the very successful models which can explain the IRAS 60  $\mu\text{m}$  counts, ISO 15  $\mu\text{m}$  counts, and cosmic far-infrared background radiation recently detected by COBE/FIRAS. At 90  $\mu\text{m}$ , the true confusion limit is one order of magnitude greater than the limit estimated

by the model at an angular resolution of  $10''$  or for a telescope diameter of 2.2 m. The model predictions of the confusion limits of HII/L2 or FIRST at both 90 and 170  $\mu\text{m}$  should be regarded as lower limits.

In Figure 5,  $5\sigma$  detection limits of a TPF like  ${}^n C_2$  interferometer ( $4 \times 3.5$  m) for telescope temperatures, 5, 10, 20, and 40 K with 5% emissivity are compared with those of NGST, HII/L2, and FIRST (Nakagawa et al. 1998). The assumed total observing time is 3600 seconds. As for the interferometer, we assume  $T = 0.1$ ,  $\sigma = 2e^-$ ,  $\Delta\nu/\nu = 0.1$ , coherent integration time  $t = 100$  seconds, and  $B = 100$  m.

In Figure 6,  $5\sigma$  detection limits of a TPF like  ${}^n C'_n$  interferometer are calculated for the same conditions.

In the near-infrared, the  ${}^n C'_n$  interferometer is more sensitive than the  ${}^n C_2$  interferometer. However the spatial resolution of NGST is sufficient and its sensitivity is superior to both interferometers for the purpose of galaxy counts. In the mid-infrared, the sensitivities of the interferometers are comparable to the sensitivity of HII/L2 though spatial resolutions are different.

The advantage of the interferometers is obvious in the far-infrared. In the present concept of TPF, the telescope temperature of 40 K is assumed. Even with 40 K telescopes, the interferometers are more sensitive than HII/L2 or FIRST at  $\lambda > 100 \mu\text{m}$ . It is clear from the performance for 5 K telescopes that an actively cooled interferometer in the far-infrared regardless of the beam combination geometry is ideal for detecting faint galaxies which are otherwise undetected due to source confusion.

#### ACKNOWLEDGMENT

TN is supported by Grant-in-Aid for Scientific Research of the Japanese Ministry of Education, Culture, Sports, and Science (No. 10640239) and by the Sumitomo Foundation.

#### REFERENCES

- Goodman, J. W. 1985, *Statistical Optics* (New York: Wiley)  
 Guiderdoni, B. et al. 1998, *MNRAS*, 295, 877  
 Kawara, K. et al. 1998, *A&A*, 336, L9  
 Matsuhara, H. et al. 2000, *A&A*, 361, 407  
 Nakagawa, T. et al. 1998, *SPIE Proc.*, 3356, 462  
 Penny A. J. et al. 1998, *SPIE Proc.*, 3350, 666  
 Prasad, S., & Kulkarni, S. R. 1989, *JOSA*, A6, 1702  
 Puget, J. L. et al. 1999, *A&A*, 345, 29  
 The TPF Science Working Group, ed. Beichman C. A., Woolf, N. J., & Lindensmith, C. A. 1999, *TPF: Terrestrial Planet Finder, Origins of Stars, Planets and Life*, JPL Publication 99-003 (Pasadena: JPL)  
 Walkup J. F. & Goodman J. W. 1973, *JOSA*, 63, 399